GeroScience (2023) 45:931–948
https://doi.org/10.1007/s11357-022-00692-3

ORIGINAL ARTICLE

Recapitulation of anti-aging phenotypes by global, but not by muscle-specific, deletion of PAPP-A in mice

Xinna Li · Mary Hager · Madaline McPherson · Michael Lee · Riha Hagalwadi · Mary E. Skinner · David Lombard · Richard A. Miller

Received: 18 May 2022 / Accepted: 15 November 2022 / Published online: 21 December 2022

Abstract Deletion of pregnancy-associated plasma protein-A (PAPP-A), a protease that cleaves some but not all IGF1 binding proteins, postpones late-life diseases and extends lifespan in mice, but the mechanism of this effect is unknown. Here we show that PAPP-A knockout (PKO) mice display a set of changes, in multiple tissues, that are characteristic of other varieties of slow-aging mice with alterations in GH production or GH responsiveness, including Ames dwarf, Snell dwarf, and GHRKO mice. PKO mice have elevated UCP1 in brown and white adipose tissues (WAT), and a change in fat-associated macrophage subsets that leads to diminished production of inflammatory cytokines. PKO mice also show increased levels of muscle FNDC5 and its cleavage product, the myokine irisin, thought to cause changes in fat cell differentiation. PKO mice have elevated production of hepatic GPLD1 and plasma GPLD1, consistent with their elevation of hippocampal BDNF and DCX, used as indices of neurogenesis. In contrast, disruption of PAPP-A limited to muscle ("muPKO" mice) produces an unexpectedly complex set of changes, in most cases opposite in direction from those seen in PKO mice. These include declines in WAT UCP1, increases in inflammatory macrophages and cytokines in WAT, and a decline in muscle FNDC5 and plasma irisin. muPKO mice do, however, resemble global PKO mice in their elevation of hippocampal BDNF and DCX. The data for the PKO mice support the idea that these changes in fat, macrophages, liver, muscle, plasma, and brain are consistent and biologically significant features of the slow-aging phenotype in mice. The results on the muPKO mice provide a foundation for further investigation of the complex, local, and global circuits by which PAPP-A modulates signals ordinarily controlled by GH and/or IGF1.

Keywords Pregnancy-associated plasma protein-A (PAPP-a) · Uncoupling protein 1 (UCP1) · Fibronectin type III domain-containing protein 5 (FNDC5)/IRISIN · Glycosylphosphatidylinositol-specific phospholipase D1 (GPLD1) · Brain-derived neurotrophic factor (BDNF) · Doublecortin (DCX)

Supplementary Information The online version contains supplementary material available at https://doi.org/10.1007/s11357-022-00692-3.

X. Li (✉) · M. E. Skinner · D. Lombard · R. A. Miller
Department of Pathology, University of Michigan School of Medicine, Ann Arbor, MI 48109, USA
e-mail: xinna@umich.edu

X. Li
Ann Arbor, USA

M. Hager · M. McPherson · M. Lee · R. Hagalwadi
College of Literature, Sciences, & the Arts, University of Michigan, Ann Arbor, MI 48109, USA

D. Lombard
Sylvester Cancer Center, University of Miami Miller School of Medicine, Miami, FL 33136, USA

R. A. Miller
University of Michigan Geriatrics Center, Ann Arbor, MI 48109, USA

Introduction

Pregnancy-associated plasma protein-A (PAPP-A) is a protease that cleaves some of the IGF1 binding proteins in mice, and in this way is thought to regulate effective concentration of IGF1 in multiple tissues [1]. Disruption of PAPP-A in PAPP-A-KO mice ("PKO" mice) leads to a 20–40% increase in lifespan compared to wild-type (WT) control littermates [2–4]. Inhibition of IGF1-mediated signaling causes proportional dwarfism in PKO mice during the beginning of embryogenesis before organogenesis [1]. Biological processes regulated by IGF over the course of puberty and early adulthood are also affected in PKO mice, resulting in decreased bone mass and ovarian steroidogenesis compared to WT littermates [5, 6]. Altered glucose–insulin homeostasis and decreased energy expenditure were found not to be factors in the increased longevity of PKO mice, and circulating levels of IGF1 in PKO mice are similar to those in wild-type littermates [7]. Evaluations of expression of genes related to IGF1 and IGF2 responses were altered in heart, liver, and kidney of PKO mice, with parallel changes in the corresponding tissues of long-lived Snell dwarf mice, in which circulating IGF1 is reduced [8]. PKO mice are resistant to the development of atherosclerosis, show delay in age-dependent thymic atrophy, and have delayed cancer development [3, 9]. PKO mice are also resistant to the development of diabetic nephropathy [10].

Uncoupling protein 1 (UCP1) was first identified as a 32,000 M_r cold-inducible protein in brown adipose tissue [11]. It plays a crucial role in thermogenesis by uncoupling oxidative phosphorylation [12, 13]. Clusters of UCP1-expressing adipocytes in white adipose tissue (WAT) increase in response to cold stimulation or β3-adrenergic receptor agonists [14–16]. These adipocytes have been termed beige, "brite" (brown in white), iBAT (induced BAT), recruitable BAT, and wBAT (white adipose BAT) [17]. These beige cells have a common ability to undergo thermogenesis [18]. Brown and beige cells differ in many ways and are considered distinct cell types [19, 20].

Adipose tissue is also immunologically active [21]. Macrophages play an important role in the inflammatory response of adipose tissue [22]. Macrophages can be divided into pro-inflammatory M1 type (classically activated macrophage) and anti-inflammatory M2 type (alternatively activated macrophage), although cells with intermediate phenotypes exist as well [23, 24]. M1 macrophages secrete pro-inflammatory cytokines and chemokines, such as such as TNF-α, interleukin IL-6, and MCP-1, promoting many kinds of protective immune responses [25]. In contrast, M2 macrophages mainly secrete arginase-1, IL-10, IL-4, and other anti-inflammatory cytokines, which reduce inflammation [25–28] and protect against tissue damage. Adipose tissue inflammation, characterized by increased macrophage infiltration and polarization from the M2 to the pro-inflammatory M1 phenotype, plays an important role in obesity-induced chronic systemic inflammation and insulin resistance [28]. Low-grade adipose tissue inflammation is also characteristic of aging in humans and in rodents [29–31], and M1/M2 macrophage polarization provides an index of this age-related inflammation [32, 33].

FNDC5, a transmembrane protein, was first characterized in 2002 [34, 35]. In response to exercise, FNDC5, a PGC-1α-dependent myokine, is cleaved and secreted as irisin. Irisin acts in WAT to promote fat browning by conversion of white adipose tissue (WAT) to brown adipose tissue (BAT) [36]. FNDC5 is expressed in multiple tissues including heart, brain, ovary, testis, kidney, stomach, and liver in addition to skeletal muscle [37]. Irisin reduces levels of pro-inflammatory cytokines (TNFα, IL-1β, IL-6, MCP-1) and promotes secretion of anti-inflammatory cytokines (IL-10, IL-4, IL-13) in adipose tissue [38–40].

Brain-derived neurotrophic factor (BDNF) belongs to a family of neurotrophins that have a crucial role in survival and differentiation of neuronal populations during development [41]. The microtubule-associated protein doublecortin (DCX) is expressed widely in neuronal precursor cells, immature neurons, and migrating neurons throughout the developing and adult nervous system [42, 43], and an increase in DCX is thus considered a sign of increased neurogenesis. Age-dependent impairment in cognitive function is associated with decreases in BDNF and DCX expression in the primary regions of the brain [44–46].

We have begun to define sets of traits, in multiple organs, that distinguish various kinds of slow-aging mice from their controls. In a study of Snell dwarf ($Pit1^{dw/dw}$) and growth hormone receptor (GHR) knockout ("GHRKO") mice, for example [47], we noted upregulation of uncoupling protein 1 (UCP1) in brown adipose tissue (BAT) and in three depots of white adipose tissue (WAT) including inguinal, perigonadal, and mesenteric fat. We also noted conversion of

adipocytes in WAT to the brown/beige cell type characterized by smaller size, increased cytoplasm, and increased mitochondrial number. This conversion of WAT adipocytes was accompanied by a decline in the number of pro-inflammatory M1 macrophages and a corresponding increase in the number of anti-inflammatory M2 macrophages, along with lower mRNA levels of three inflammatory cytokines produced by M1 cells. Disruption of GHR in liver did not replicate any of these changes, implying that the changes were unlikely to be due to decline in GH-dependent secretion of IGF1 by the liver. Similarly, depletion of GHR in fat tissue did not reproduce any of these changes, implying that the effects on fat cells and on fat-associated macrophage populations were dependent on GH-dependent status in some other tissue. In contrast, disruption of GHR in skeletal muscle did replicate most of the changes, in fat cells and in fat-associated macrophages of Snell and global GHRKO mice [47], suggesting that some GH-regulated myokine was implicated in these effects. We then noted an increase, in Snell, GHRKO, and muscle-specific GHRKO, in serum irisin, previously implicated [47] in signaling muscle status to fat tissue as a consequence of exercise. Irisin did not, however, increase in mice where GHR was disrupted in liver or fat cells. FNDC5, the muscle protein of which irisin is a cleavage product, was also shown to be increased in Snell, global GHRKO, and muscle-specific GHRKO mice. This suggested a model in which low GH signals in muscle of the long-lived Snell and GHRKO mice led to increased muscle FNDC5, increased plasma irisin, increased white-to-brown fat conversion, and alterations in the balance between M1 and M2 macrophages.

In a separate study, we have extended the analysis of Snell and GHRKO mice to show an increase, in both kinds of mice, in production of the liver protein GPLD1 [48]. Others have shown that when mice exercise, their livers secrete a protein called GPLD1 (glycosylphosphatidylinositol (GPI)-degrading enzyme) into the blood. When GPLD1 was overexpressed in liver of young adult mice, plasma GPLD1 increased, and the animal showed improvements in cognition and memory, and increased hippocampal neurogenesis within 3 weeks [49]. This group found that GPLD1 produced by the liver does not pass through the blood–brain barrier. The mechanism by which plasma GPLD1 modulates cell physiology and function in the central nervous system is not known, but may involve pathways that reduce inflammation and blood coagulation throughout the body [49]. In our work, we noted elevation of GPLD1 protein in liver and in plasma of Snell dwarf and GHRKO mice. Interestingly, the elevation of liver GPLD1 protein in these long-lived mutant mice was not accompanied by any change in mRNA level, suggesting that the increase in GPLD1 protein reflected alterations in mRNA translation or protein stability. GPLD1 was also elevated, in culture and in mice, by a drug that induces translation of mRNAs via cap-independent translation (CIT), and was increased in liver of mice carrying a YTHDF1 transgene that also induces CIT. This evidence indicates that the increase in GPLD1 in Snell and GHRKO mice reflects the general increase of CIT activity in these long-lived mice [50, 51]. Induced over-expression of GPLD1 has been shown, in mice, to produce increased neurogenesis, as indicated by levels of doublecortin (DCX) in hippocampus, and to increased levels of brain-derived neurotrophic factor (BDNF). Our own work [48] has established that Snell and GHRKO mice did indeed have higher levels of DCX and BDNF in hippocampus, consistent with their higher plasma levels of GPLD1.

The current investigation began as an evaluation of the extent to which these changes in adipocytes, macrophages, skeletal muscle, liver, plasma, and brain, which are seen in Snell and GHRKO mice, were also characteristic of PKO mice, presumed to have diminished levels of PAPP-A in multiple tissues. The data presented below show that this suite of phenotypic changes is replicated almost entirely in PKO mice. To test whether deletion of PAPP-A in muscle alone might lead to parallel alterations in multiple tissues, we also created and studied mice in which PAPP-A was disrupted in skeletal muscle only, and noted a remarkable, and in many cases, paradoxical set of changes that, taken together, suggest a complex set of unsuspected feedback loops contingent on tissue-specific PAPP-A effects.

Materials and methods

Mice

Breeding stock for PKO mice was provided by Cheryl Conover (Mayo Clinic, Rochester, MN) and mice were

produced as previously described [1, 52]. PKO mice were used at ages from 5 to 6 months, and heterozygous littermates were used as controls. All experiments were approved by the University of Michigan Institutional Animal Care and Use Committee. Mice used were fed ad lib.

Generation of muscle-specific PKO mice (muPKO model)

Transgenic mice hemizygous for B6.FVB(129S4)-Tg(Ckmm-cre)5Khn/J, a Cre recombinase with skeletal and cardiac muscle–specific expression driven by the muscle creatine kinase promoter (MCK-Cre), were purchased from The Jackson Laboratory (Strain 006,475) and crossed to homozygous PAPP-A floxed mice (fPAPP-A) [52]. Progeny were bred to homozygous fPAPP-A mice to generate offspring that were homozygous for fPAPP-A and either Cre negative or hemizygous MCK-Cre positive. To assess the degree of specificity of PAPP-A disruption in muPKO mice, we evaluated the level of the excised PAPPA sequence in four male Cre-positive (knockout) and four Cre-negative (control) mice, using muscle, liver, hippocampus, brown adipose tissue, inguinal fat, and perigonadal fat. Muscle from all four Cre-positive mice showed a band at the expected size of the excised PAPPA sequence, and this excision band was absent from all other tissues in the mice tested, and absent from all tissues from the non-mutant mice. We conclude that the mutant does, as expected, lead to disruption of the PAPPA sequence in muscle but not in any of the other 5 tested tissues. Sex-matched littermates with and without MCK-Cre were selected for analysis at 80–100 days of age.

Genotyping of mice and tissues

To identify experimental mice, DNA from tail snips was obtained for PCR. Generic Cre primers were 5′-CAAAACAGGTAGTTATTCGG-3′ (forward) and 5′-CGTATAGCCGAAATTGCCAG-3′ (reverse). The PCR protocol was 94 °C for 3 min and then 94 °C for 30 s, 59 °C for 30 s, and 72 °C for 30 s for 35 cycles, and then a hold at 4 °C.

DNA isolation and PAPP-A excision PCRs in tissues of muscle-specific PAPP-A knockout mice

Tissue samples were taken from adult (4–6 months old) wild-type littermate control mice (WT) and MuPKO mice of both sexes. Samples were homogenized utilizing the Bullet Blender from Next Advance (Averill Park, NY, USA). DNA was isolated from various tissues (liver, brown adipose, inguinal adipose, perigonadal adipose, hippocampus, and muscle) of MuPKO using Mammalian Genomic DNA Miniprep kit (MilliporeSigma, Inc, Rockville, MD) according to the manufacturer's instruction. The concentration of total DNA was measured by absorbance at 260 nm by using a Nanodrop ND-100. The efficiency of PAPP-A deletion in various tissues of muPKO mice was determined by a 3-primer endpoint PCR. Primers were the following: common forward, 5′-TAGTTCCTCCAGCTTTTACCTTG-3′; intact reverse, 5′-ATTTGTCATACAGCCCTATGTG-3′; and excised reverse, 5′-AAAATGCCATAAACT ATAGGG-3′. The PCR protocol used an initial denaturization step of 95 °C for 3 min and then 32 cycles of 95 °C for 10 s, 54 °C for 30 s, a final elongation of 72 °C for 7 min, and a hold at 4 °C. End products were visualized on a 2% agarose/ethidium bromide gel. For this PCR, the WT allele will be at 200 bps, intact PAPP-A flox will be detected at 288 bps, and excised PAPP-A will be detected at 240 bps.

RNA isolation and cDNA synthesis

Tissue samples were taken from adult (4–6 months old) mice of both sexes. Samples were homogenized utilizing the Bullet Blender from Next Advance (Averill Park, NY, USA). Total RNA was isolated from mouse livers and adipose tissues using Carbon-Prep Phenol/Trizol kit (Life Magnetics, Inc, Detroit, MI) according to the manufacturer's instruction. The RNA was cleaned using the QiagenRNeasy miniRNA cleanup protocol (Qiagen, Valencia, CA). The concentration of total RNA was performed by measuring the absorbance of RNA sample solutions at 260 nm by using a Nanodrop ND-100. Total RNA (1.0 µg) was reverse transcribed using iScript cDNA reverse transcription kits (1,708,891; Bio-Rad, Hercules, CA) according to the manufacturer's instructions.

Quantitative real-time PCR

qPCR was performed using the Fast Start Universal SYBR Green Master Mix (Applied Biosystems, Foster City, CA). Reactions were performed using an Applied Biosystems 7500 Real-Time RT-PCR

System. RT-PCR was performed using quantitative PCR systems (Applied Biosystems® 7500 Real-Time PCR Systems, Thermo Fisher Scientific, Waltham, MA, USA) with corresponding primers (Table 1, Invitrogen). Glyceraldehyde-3-phosphate dehydrogenase (GAPDH) was simultaneously assayed as a loading control. The cycle time (CT) was normalized to GAPDH in the same sample. The expression levels of mRNA were reported as fold changes vs. sham control. Reactions were performed using an Applied Biosystems 7500 Real-Time RT-PCR System. Data was analyzed using a ΔΔCT approach. See Table S1 for a list of primers used.

Western blot analyses

Proteins from various tissues of the experimental mice (brown adipose, inguinal adipose, perigonadal adipose, liver, muscle, and hippocampus) were extracted after homogenization in Immunoprecipitation Assay Buffer (RIPA Buffer, Fisher Scientific, Pittsburgh, PA, USA) supplemented with Complete Protease Inhibitor Cocktail (Roche Inc.). Protein content was measured using a BCA assay (Fisher Scientific, Pittsburgh, PA, USA). The protein extracts were separated by SDS/PAGE on a 4–15% running gel, transferred to polyvinylidene difluoride membranes, and electro-transferred to an Immobilon-P Transfer Membrane (Millipore, Billerica, MA, USA) for immune blot analyses. Membranes were blocked in Tris buffered saline containing 0.05% Tween20 (TBS-T) and 5% bovine serum albumin (BSA) for 1 h. After blocking, membranes were probed overnight with primary antibodies in TBS-T supplemented with 5% BSA with shaking at 4 °C, followed by three 10-min washes with TBS-T, incubation with secondary antibody for 1 h, and three 10-min washes with TBS-T. Membranes were then evaluated using an ECL chemiluminescent substrate (Fisher Scientific, Pittsburgh, PA, USA). The following antibodies were used: anti-GPLD1 (Abcam, catalog no. 210753, 1:1000), anti-BDNF (Abcam, catalog no. 108319, 1:1000), anti-doublecortin (Abcam, catalog no. 18723, 1:1000), anti-β-actin (Santa Cruz Biotechnology, 1:1000), HRP-conjugated anti-mouse (GE Healthcare UK Limited, 1:2000), and anti-rabbit (GE Healthcare UK Limited, 1:5000). Quantification was performed using ImageJ software. Table S2 provides a list of the antibodies used.

Adipose histology

Adipose tissue was cut into small pieces, rinsed in PBS, and fixed overnight in Bouin's solution. Fixed

Table 1 Collection of statistical results of PKO and MuPKO

Tissue	Protein	*p*-value (PKO)	Direction (PKO)	*p*-value (MuPKO)	Direction (MuPKO)
Inguinal fat	UCP1	***p* < 0.001**	**Up**	***p* < 0.001**	**Down**
Perigonadal fat	UCP1	***p* < 0.001**	**Up**	***p* < 0.01**	**Down**
BAT	UCP1	***p* < 0.001**	**Up**	$p = 0.4$	**No change**
Inguinal fat	ARG1	***p* < 0.001**	**Up**	***p* < 0.001**	**Down**
Perigonadal fat	ARG1	***p* < 0.05**	**Up**	***p* < 0.01**	**Down**
BAT	ARG1	***p* < 0.01**	**Up**	$p = 0.7$	**No change**
Inguinal fat	iNOS	***p* < 0.001**	**Down**	***p* < 0.001**	**Up**
Perigonadal fat	iNOS	***p* < 0.05**	**Down**	***p* < 0.001**	**Up**
BAT	iNOS	***p* < 0.01**	**Down**	$p = 0.3$	**No change**
Muscle	FNDC5	***p* < 0.01**	**Up**	***p* < 0.01**	**Down**
Hippocampus	FNDC5	***p* < 0.001**	**Up**	***p* < 0.001**	**Up**
Liver	GPLD1	***p* < 0.01**	**Up**	***p* < 0.001**	**Down**
Hippocampus	GPLD1	$p = 0.8$	**No change**	***p* < 0.001**	**Up**
BAT	GPLD1	***p* < 0.01**	**Up**	$p = 0.5$	**No change**
Hippocampus	BDNF	***p* < 0.01**	**Up**	***p* < 0.001**	**Up**
Hippocampus	DCX	***p* < 0.001**	**Up**	***p* < 0.001**	**Up**

tissues were flushed for 10 min with tap water and stored at 4 °C in PBS, then sectioned and stained with hematoxylin–eosin.

Measurement of irisin and GPLD1 levels by enzyme-linked immunosorbent assay

Blood samples from the PKO and MuPKO mice were collected into ethylene diamine tetraacetic acid (EDTA)-coated tubes, and plasma was isolated by centrifugation (10,000 rpm, 4 °C, 10 min). ELISA kits were used to determine the levels of FNDC5/irisin (LSBio, Seattle, WA) and GPLD1 (antibodies-online INC, Limerick, PA, USA) according to the standard protocol. Briefly, serum samples from PKO and MuPKO mice were added into each well and incubated at room temperature for 120 min. Then the biotin-conjugated antibody was added, followed by incubation for 90 min. Thereafter, the substrate solution was added into the well and incubated for 30 min. After washing five times with 0.01 mol/L tris-buffered saline (TBS), 3,3′,5,5′-tetramethylbenzidine (TMB) was added and incubated for 30 min in the dark. The absorbance at 450 nm was determined using a Bio-Rad iMark microplate reader.

Statistical analysis

The data shown in each figure represent results of a minimum of three independent experiments. All data are presented as mean ± SEM. The Student's two-tailed *t*-test was used for comparisons of two experimental groups. $P < 0.05$ was regarded as significant.

Results

UCP1 protein levels in BAT and WAT of PKO and MuPKO mice. As shown in Fig. 1 (panels A, C, E), UCP1 protein levels are higher in BAT and in inguinal and perigonadal WAT of PKO mice, compared to heterozygote littermate controls. A two-factor ANOVA (sex, genotype, interaction) found no evidence for a sex-specific effect on UCP1, and so data were combined across sex, with both males and females shown in this and subsequent figures. Results of these ANOVA calculations, for each endpoint used in this report, are collected in Table S3. UCP1 protein was elevated by a factor of 1.6–2.5 in the three fat depots, in each case with $p < 0.001$ for the *t*-test comparison to controls. Tissue sections, shown in Fig. S1, show that BAT and WAT undergo transitions in cell size and structure consistent with the upregulation of UCP1 and conversion of white to beige adipose tissue, as previously noted in Snell and GHRKO mice.

We found, as expected, that MuPKO mice showed disruption of the PAPPA sequence in muscle but not in liver, brown adipose, inguinal adipose, perigonadal adipose, or hippocampus (Supplemental Fig. S2). In contrast to the mice with global deletion of PAPPA, MuPKO mice exhibit a dramatically different set of changes in adipose tissue. The increase in UCP1 seen in BAT of PKO mice is absent from MuPKO (Fig. 1, panel B; mutant/control ratio of 0.9, $p = 0.4$). In the WAT of MuPKO mice, UCP1 is significantly lower than in controls (ratio 0.7 and $p < 0.01$ for perigonadal fat; ratio 0.7 and $p < 0.001$ for inguinal fat), i.e., opposite in direction to that seen in fat of global PKO mice (Fig. 1, panels D and F).

Evaluation of mRNA levels of UCP1 in PKO and MuPKO mice is collected in Fig. S3, panel A, and shows patterns quite consistent with the data on UCP1 protein, i.e., elevated mRNA in WAT and BAT of PKO mice, decline in UCP1 mRNA in WAT of MuPKO, and no change in BAT of MuPKO animals. The mRNA data thus support the immunoblotting results of Fig. 1 and suggest that the changes in UCP1 protein caused by PAPP-A genotype are likely to reflect transcriptional regulation. Table 1 collects the fold-change and *p*-value calculations for these endpoints, and for all the other endpoints presented in this report.

Shift in macrophage subsets from inflammatory to anti-inflammatory status. We used Arg1 (Fig. 2) as an index of M2 macrophages and iNOS (Fig. 3) as an index of inflammatory macrophages, chosen from a broader panel of markers employed in our previous work on Snell and GHRKO mice [47]. Arg1 is elevated in BAT, in inguinal WAT, and in perigonadal WAT of PKO mice (Fig. 2, panels A, C, E), by factors of 1.4- to 1.7-fold. Conversely, iNOS is diminished significantly in each of these three PKO tissues (Fig. 3, panels A, C, E), to levels 60–70% of those in heterozygous control mice; see Table 1 for a compilation of these statistics. By contrast, in MuPKO mice, BAT shows no alteration in Arg1 or iNOS levels. Inguinal and perigonadal WAT depots do

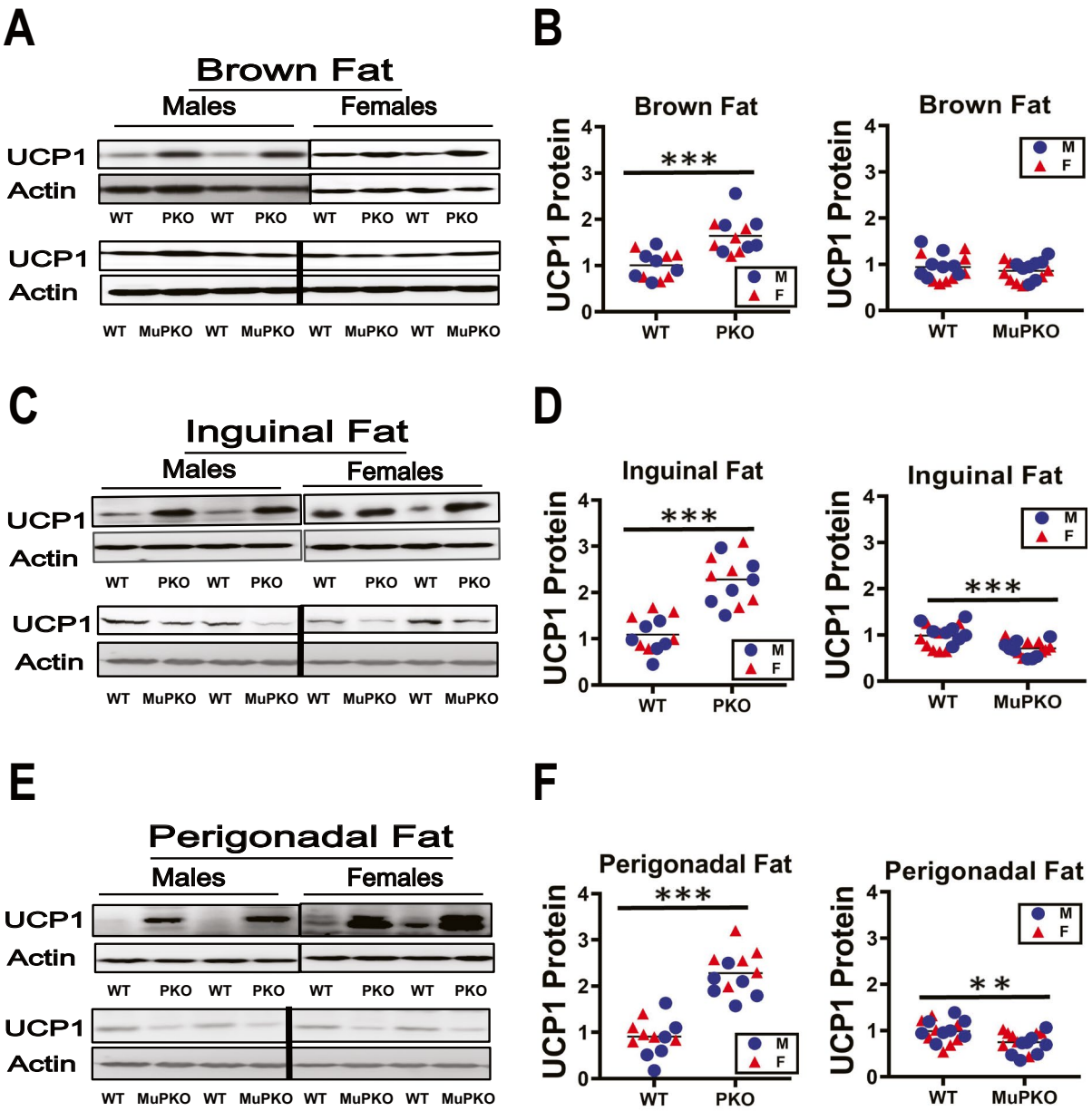

Fig. 1 Expression of UCP1 in adipose tissue of PAPP-A knockout mice (PKO) and muscle specific PAPP-A knockout mice (MuPKO). **A**, **C**, **E** Cell lysates were prepared from adipose tissues of 24-week-old wild-type littermate control mice (WT), PKO mice, and MuPKO mice. Protein levels of UCP1 (brown and beige fat marker) were measured by western blotting. Representative gel images showing UCP1 in brown adipose tissue (**A**), inguinal adipose tissue (**C**), and perigonadal adipose tissue (**E**). **B**, **D**, **F** Protein quantification data normalized to β-actin and expressed as fold change compared with WT control (defined as 1.0). $N=6$ mice for each group (WT and PKO). $N=8$ mice for each group (MuPKOWT and MuPKO). Data are means ± SEM. ** $P<0.01$, *** $P<0.001$ versus WT

show significant changes, but they are opposite in direction to those noted in global PKO mice for both Arg1 and iNOS (Figs. 2 and 3; panels B, D, F). This pattern thus matches precisely that seen for UCP1 in both mouse models. Data on mRNA encoding Arg1 and iNOS (Fig. S3, panels B and C) are fully consistent with the protein data

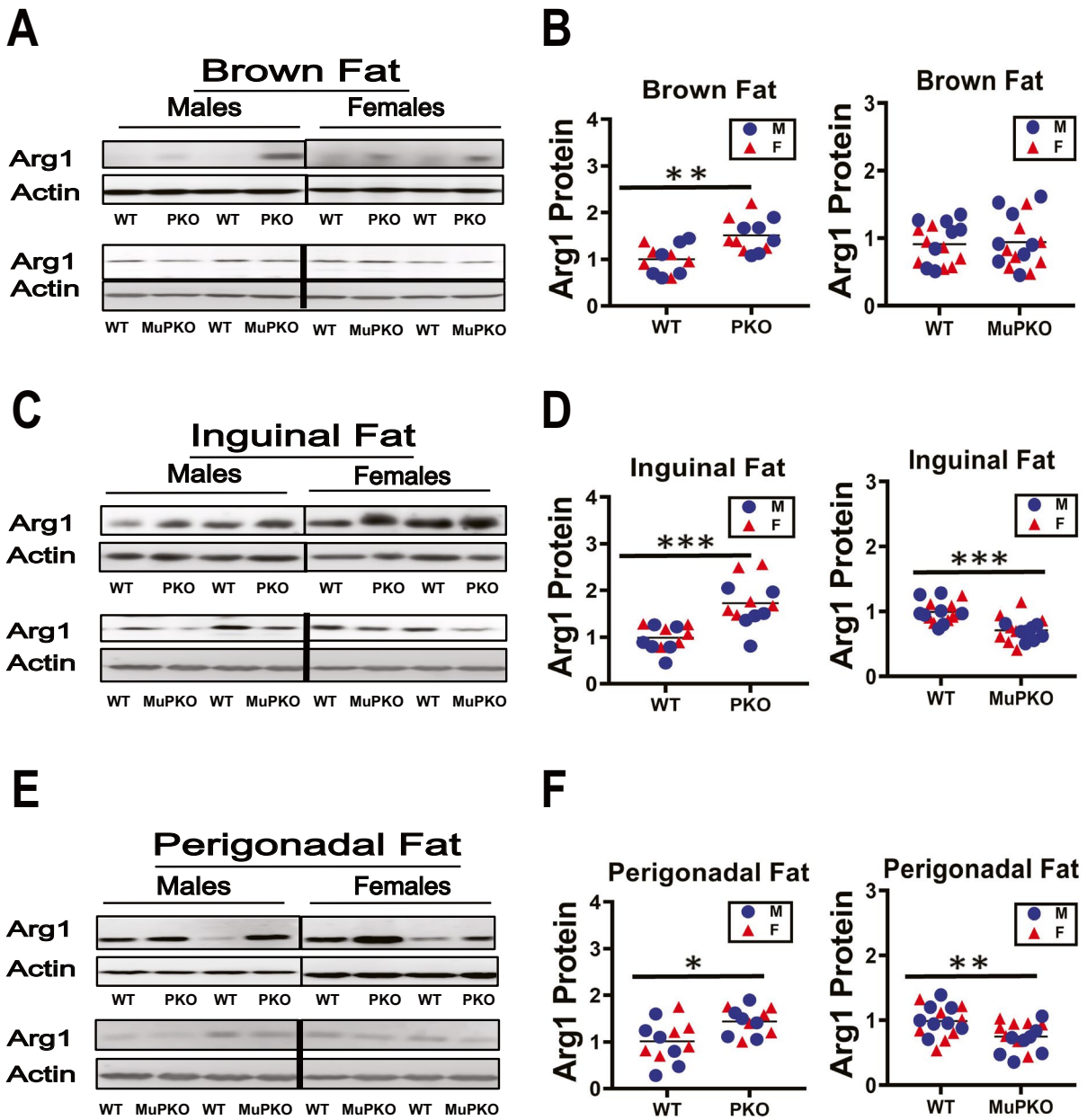

Fig. 2 Effects of PKO and MuPKO on inguinal adipose tissue macrophage infiltration and M2 macrophage marker. **A**, **C**, **E** Cell lysates were prepared from adipose tissues of 24-week-old wild-type littermate control mice (WT), PKO mice, and MuPKO mice. Protein levels of Arg1 (M2 macrophage marker) were then measured by western blotting. Representative gel images showing UCP1 in brown adipose tissue (**A**), inguinal adipose tissue (**C**), and perigonadal adipose tissue (**E**). **B**, **D**, **F** Protein quantification data normalized to β-actin and expressed as fold change compared with WT control (defined as 1.0). $N=6$ mice for each group (PKOWT and PKO). $N=8$ mice for each group (MuPKOWT and MuPKO). Data are means ± SEM. ** $P<0.05$, ** $P<0.01$, *** $P<0.001$ versus WT

in both kinds of mice, supporting the conclusions from the immunoblotting and suggesting an important role for transcriptional control of expression of these proteins.

Consistent with the data on M1 macrophages, we also noted decreased levels of mRNA for IL6, TNFα, and MCP1 in BAT and both WAT depots of PKO mice

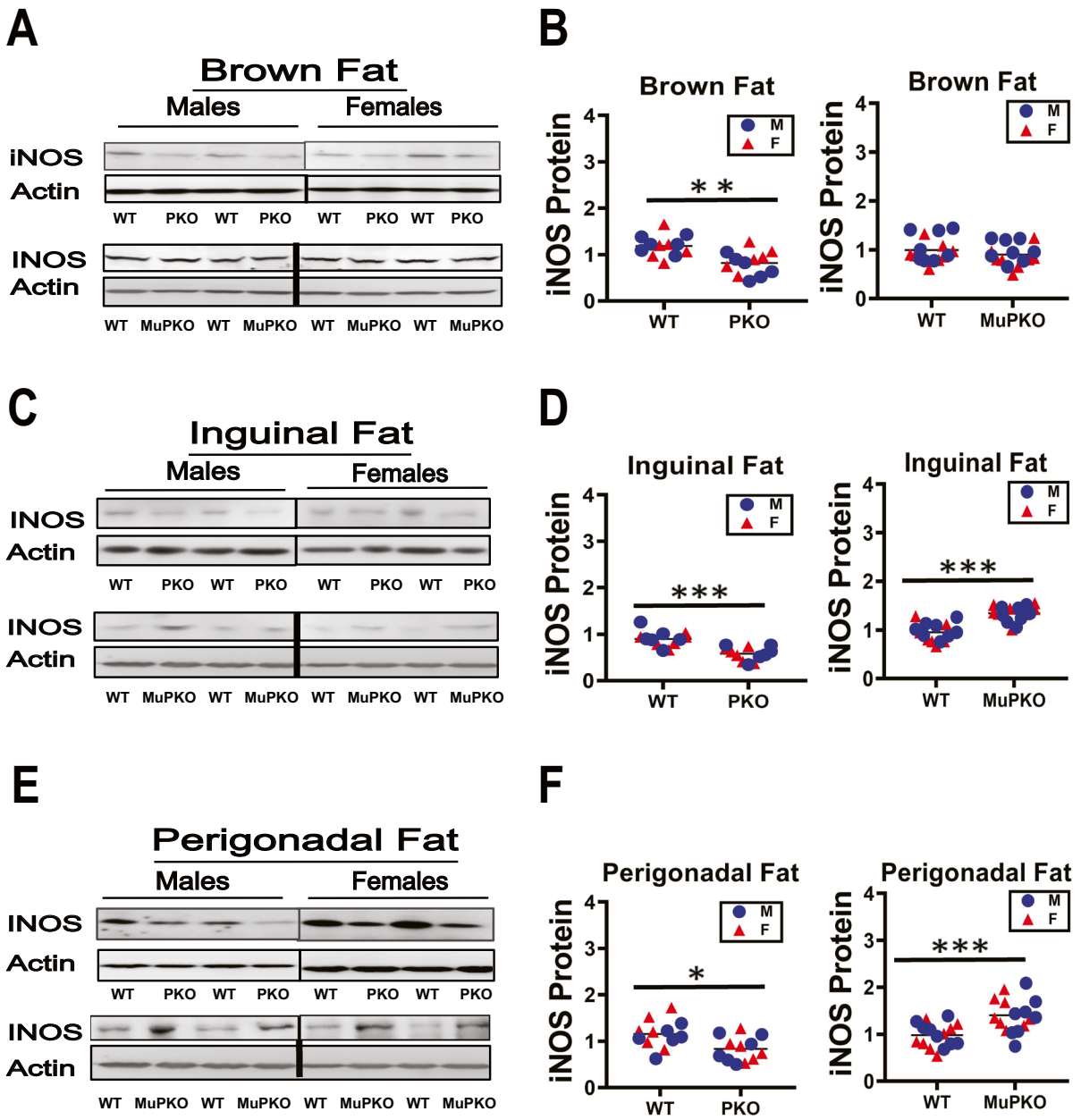

Fig. 3 Effects of PKO and MuPKO on inguinal adipose tissue macrophages. **A**, **C**, **E** Cell lysates were prepared from adipose tissues of 24-week-old wild-type littermate control mice (WT), PKO mice, and MuPKO mice. Protein levels of iNOS (M1 macrophage marker) were then measured by western blotting. Representative gel images showing UCP1 in brown adipose tissue (**A**), inguinal adipose tissue (**C**), and perigonadal adipose tissue (**E**). **B**, **D**, **F** Protein quantification data normalized to β-actin and expressed as fold change compared with WT control (defined as 1.0). $N=6$ mice for each group (PKOWT and PKO). $N=8$ mice for each group (MuPKOWT and MuPKO). Data are means ± SEM. ** $P<0.05$, ** $P<0.01$, *** $P<0.001$ versus WT

(Fig. S4). Conversely, IL6 and TNFα mRNA were significantly elevated in WAT depots of MuPKO mice, although MCP1 did not show any effects of the MuPKO mutation. There were no significant changes in any of these cytokine mRNAs in BAT of MuPKO mice, consistent with the absence of effect on iNOS levels.

Muscle FNDC5 and plasma irisin changes consistent with the alterations of adipose tissue. In our previous study [47], we found evidence for elevations of muscle FNDC5, and of its cleavage product irisin, in plasma of GHRKO and Snell mice. These effects were also seen in mice with muscle-specific GHR disruption. Figure 4 shows that muscle FNDC5 is 50% higher in PKO mice than in controls, and 50% lower in MuPKO mice compared to their own littermates, each significant at $p<0.01$. Plasma irisin (Fig. 4, panels E, F) shows the same pattern of results, with elevation in PKO and decline in MuPKO mice. In the context of our previous data from muscle-specific GHRKO mice, these observations provide a plausible explanation for the changes in UCP1 and macrophage changes seen in adipose tissues of the PKO and MuPKO animals.

We also evaluated FNDC5 in hippocampal tissues of these mice. FNDC5 is highly expressed in the brain [34, 53, 54]. It plays an important role in neuron development, and knockdown of FNDC5 in neuronal precursors impairs their development into mature neurons [54]. Recent data suggest that increased FNDC5 levels can improve cognitive function in mice [55]. PKO mice had higher levels of FNDC5 in brain, consistent with the results in skeletal muscle. Although, as noted above, muscle of MuPKO mice had lower levels of FNDC5 than controls, hippocampal FNDC5 was higher in MuPKO animals, similar to the levels seen in global PKO mice (1.8-fold higher, $p<0.001$) (Fig. 4, panels C, D). It is not known whether the genetic and neuroendocrine signals that regulate FNDC5 in brain overlap with those that affect muscle tissue, but the differences between the pattern in PKO mice (elevation in both tissues) and the results in MuPKO mice (down in muscle but up in hippocampus) strongly suggest local effects of IGF1 and IGFBPs with specific effects in hippocampus. The muscle FNDC5 results are consistent with the adipose tissue UCP1, Arg1, and iNOS data in both kinds of mice, but the hippocampal data are inconsistent in the MuPKO mice.

GPLD1 levels in tissues and plasma of global and muscle-specific PKO mice. We have previously noted elevated plasma and liver GPLD1 protein levels in Snell and GHRKO mice [48], and predicted that these would also be elevated in PKO mice. Figure 5 (panels A and B) shows that GPLD1 protein is indeed 40% higher in PKO mice than in controls, but, paradoxically, it is significantly lower (by 40%) in liver of MuPKO animals. Plasma levels of GPLD1 protein, shown in Fig. 6 (panels A and B), are consistent with the liver protein levels, i.e., higher in PKO but lower in MuPKO.

In the Snell and GHRKO mice, GPLD1 protein is also detected in hippocampus, but at levels not different from those of control mice [48]. Hippocampal GPLD1 is, as expected, unaffected by the PKO mutation (Fig. 5, panels C and D), but in contrast is significantly elevated, twofold ($p<0.001$) in MuPKO mice. GPLD1 is also increased in the brown fat of the PKO mice, similar to the effect seen in liver, but is unaltered in BAT of MuPKO mice, despite the decline of liver GPLD1 in these mice (Fig. 5, panels E and F). Thus, plasma GPLD1 levels show the same pattern of change seen in liver, which are different from the GPLD1 levels of BAT and hippocampus in both PKO and MuPKO mice, consistent with the idea that plasma GPLD1 may principally reflect production of this protein by the liver.

The idea that CIT might be responsible for elevated hepatic GPLD1 protein levels in the Snell and GHRKO mice emerged from the lack of genotype effects on GPLD1 mRNA in these two kinds of mice, prompting measurements of mRNA in the PKO animals as well. As shown in Fig. 6 (panel C), there are no differences in GPLD1 mRNA between PKO and heterozygous control mice in liver, hippocampus, or BAT, consistent with our prior data showing control of this protein by selective, cap-independent mRNA translation.

BDNF and DCX elevation in hippocampus of PKO and MuPKO mice. Because GPLD1 in plasma has been shown to increase BDNF and DCX in brain [49], and because these two proteins are increased in hippocampus of Snell and GHRKO mice [48], we expected to find both proteins elevated in brain of PKO but not in MuPKO mice. Both proteins are indeed at significantly higher levels (1.3 to 1.4 times increase, $p<0.01$) of PKO mice, as shown in Fig. 7 (panels A, B, C, D). Surprisingly, they are also elevated, by twofold and 1.4-fold, respectively, in hippocampus of MuPKO mice (panels A, B, C, D; $p<0.001$ in each case).

Discussion

It is not known why PKO mice are long lived. The predominant theory focuses on a possible role of

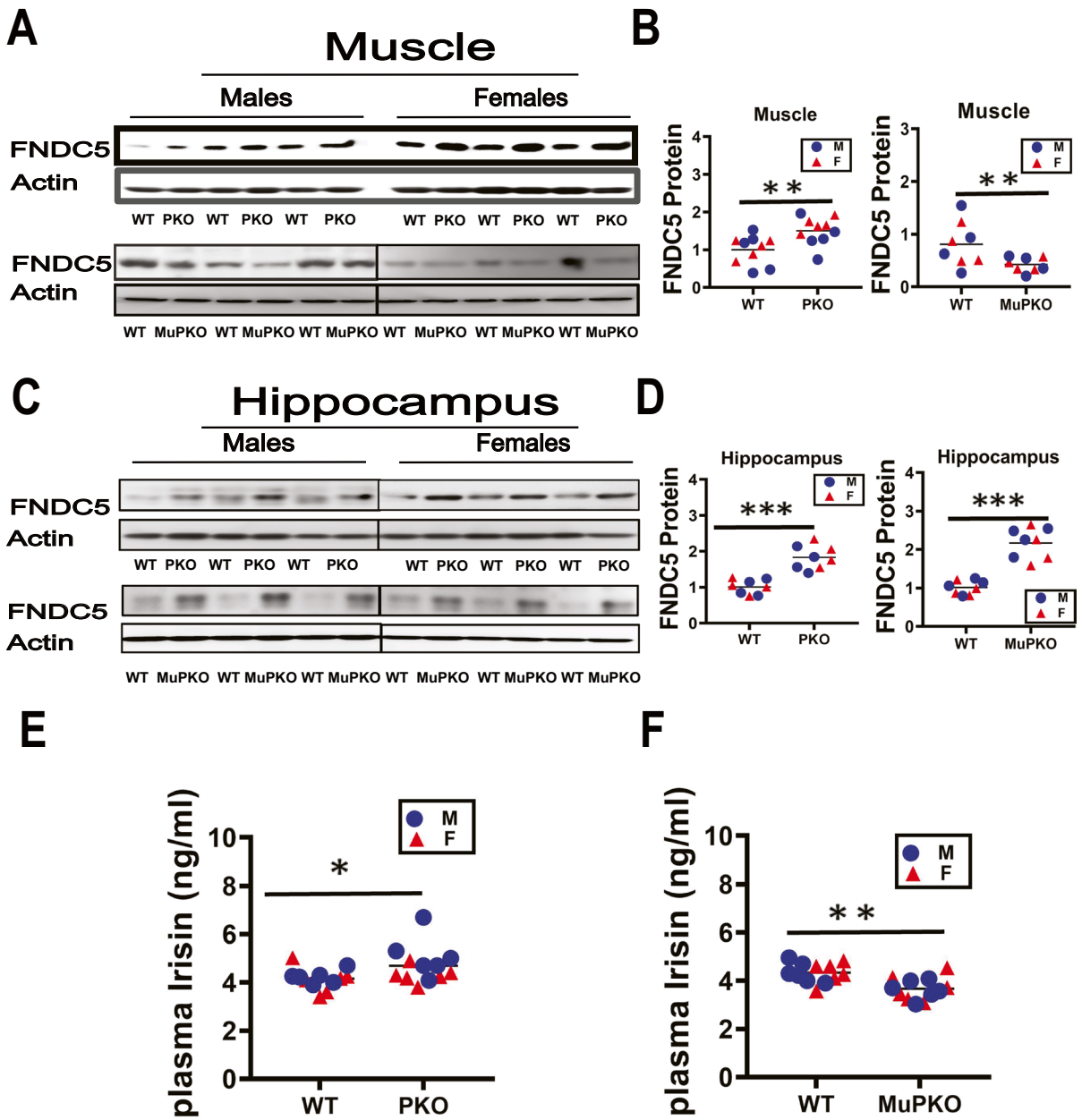

Fig. 4 Expression of FNDC5 in gastrocnemius muscle and hippocampus of PKO and MuPKO mice. **A** Cell lysates were prepared from gastrocnemius muscle of 24-week-old wild-type littermate control mice (WT), PKO mice, and MuPKO mice. Protein levels of FNDC5 were measured by western blotting. Representative gel images are shown. **B** Protein quantification data normalized to β-actin and expressed as fold change compared with WT control (defined as 1.0). $N=5$ mice for each group (PKOWT and PKO). $N=4$ mice for each group (MuPKOWT and MuPKO). Data are means ± SEM. ** $P<0.01$ versus WT. **C** Representative gel images showing FNDC5 in hippocampus. **D** Protein quantification data for hippocampus. $N=4$ mice for each group (PKOWT and PKO and MuPKOWT and MuPKO). Data are means ± SEM. *** $P<0.001$ versus WT. **E** Irisin content measured by ELISA assay on plasma samples of 24-week-old wild-type littermate control mice (WT) and long-lived mice (**PKO**). Data are shown as mean ± SEM for each group ($n=6$). * $P<0.05$ for genotype effect by two-way ANOVA. **F** Irisin content was measured by ELISA assay on plasma samples of 24-week-old wild-type littermate control mice (WT) and muscle specific PAPP-A knockout mice (MuPKO). Data are shown as mean ± SEM for each group ($n=6$). ** $P<0.01$ for genotype effect by two-way ANOVA

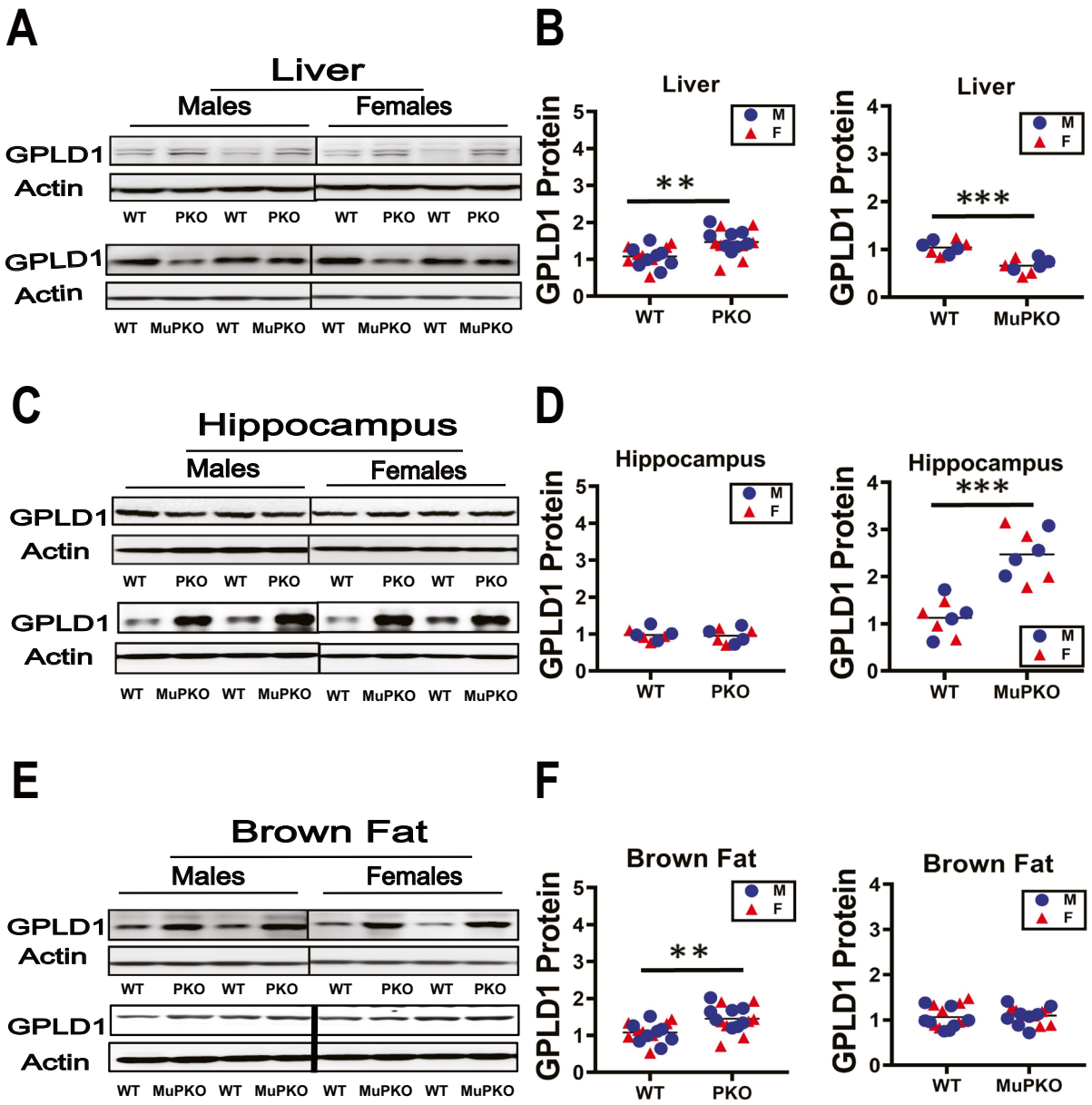

Fig. 5 Effects of PKO and MuPKO on GPLD1 in liver, hippocampus, and brown adipose tissue. **A**, **C**, **E** Cell lysate was prepared from liver, hippocampus, and brown adipose tissues of 24-week-old wild-type littermate control mice (WT), PKO mice, and MuPKO mice. Protein levels of GPLD1 were then measured by western blotting. Representative gel images showing GPLD1 in liver tissue (**A**), hippocampus tissue (**C**), and brown adipose tissue (**E**). **B**, **D**, **F** Protein quantification data normalized to β-actin and expressed as fold change compared with WT control (defined as 1.0). $N = 4–8$ mice for each group. ** $P < 0.01$, *** $P < 0.001$ versus WT

reduced IGF1 signaling, because PAPP-A is known to cleave at least two IGF binding proteins and because Ames, Snell, GHRKO, and other mutant mice with low GH levels of GH receptors exhibit low plasma IGF1 levels. The prevailing model suggests that global removal of PAPP-A would, in some unknown tissue(s), shift the balance between free IGF1- and IGF-binding proteins to diminish IGF1-dependent

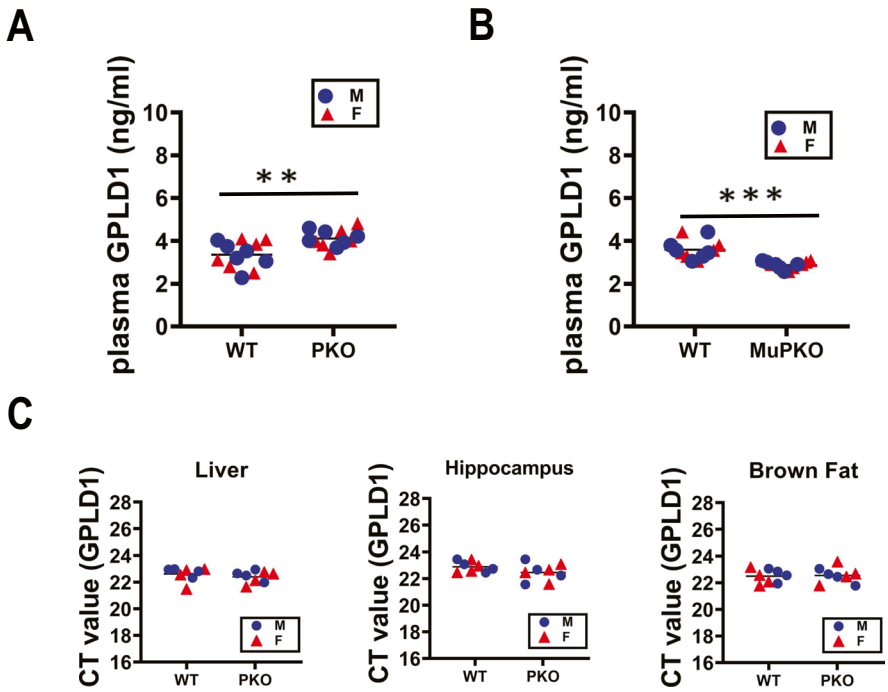

Fig. 6 Effects of PKO and MuPKO on mRNA levels of GPLD1 in liver, hippocampus, and brown adipose tissue. **A** GPLD1 protein was measured by ELISA assay on plasma samples of 24-week-old wild-type littermate control mice (WT) and long-lived mice (PKO). Data are shown as mean ± SEM for each group ($n = 6$). ** $p < 0.01$ for genotype effect by two-way ANOVA. **B** GPLD1 content was measured by ELISA assay on plasma samples of 24-week-old wild-type littermate control mice (WT) and muscle specific PAPP-A knockout mice (MuPKO). Data are shown as mean ± SEM for each group ($n = 6$). *** $P < 0.001$ by two-way ANOVA. **C** Total RNAs were isolated from liver, hippocampus, and brown adipose tissues of 24-week-old wild-type littermate control mice (WT) and PKO mice. mRNA levels of *GPLD1* were measured by qRT-PCR. Data (mean ± SEM; $n = 4$) were normalized by the amount of *GAPDH* mRNA and expressed relative to the corresponding male WT value. *$P < 0.05$ versus WT

signaling in one or more unknown cell types, with beneficial effects on health and lifespan through pathways to be determined. The details through which these IGF1-dependent events are controlled, and by which they lead to health benefits, await discovery. It is also possible that PAPP-A deficits slow aging by routes that are not related to the effects of this enzyme on IGF1 action.

This study was motivated by our recent work showing a set of traits shared by long-lived Snell, Ames, and GHRKO mice, including changes in adipocyte differentiation, macrophage polarization, myokine production, hepatic secretion of GPLD1 regulated by CIT, and two indices of brain health ([47]; Li et al. submitted). All of these changes were, in the current data set, replicated in the PKO mice (see Table 1 for summary). It seems plausible, but unproven, that the alterations in UCP1 and other regulators of adipocyte activity could lead to favorable metabolic status in long-lived mice [47], and plausible that changes in macrophage balance, with lower production of inflammatory cytokines, might retard some aspects of late-life disease. Moreover, increased levels of DCX and BDNF might contribute to the documented increase in late-life neurogenesis in Ames mice [56] and to the documented delay in age-dependent loss of cognitive function in Ames and GHRKO mice [57, 58]. We have also found that this set of changes, in fat, liver, muscle, macrophages, plasma, and brain, is characteristic of Ames dwarf mice, and can be prevented by transient exposure of Ames mice to GH injections from 2 to 8 weeks of age [59].

We note that these changes are apparent in healthy young adult mice in three of the genotypes (Snell, PKO, and GHRKO). They thus do not represent any retardation of age effects on the endpoints we have

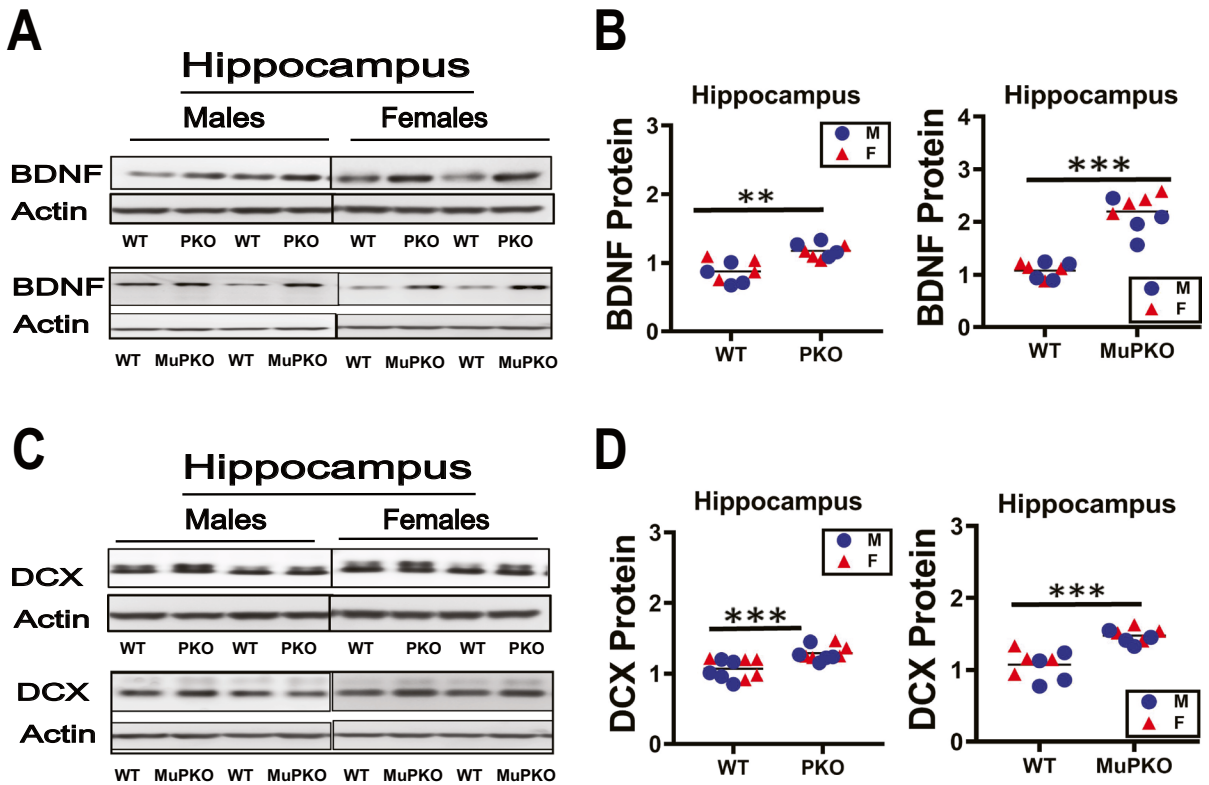

Fig. 7 Expression of BDNF and doublecortin (DCX) in hippocampus of PKO and MuPKO mice. **A** Cell lysates were prepared from hippocampus of 24-week-old wild-type littermate control mice (WT), PKO mice, and MuPKO mice. Protein levels of BDNF were measured by western blotting. Representative gel images are shown. **B** Protein quantification data normalized to β-actin and expressed as fold change compared with WT control (defined as 1.0). $N=4$ mice for each group (PKOWT and PKO). $N=4$ mice for each group (MuPKOWT and MuPKO). Data are means ± SEM. ** $P<0.01$, *** $P<0.001$ versus WT. **C** Representative gel images showing doublecortin (DCX) in hippocampus. **D** Protein quantification data for hippocampus. $N=5$ mice for each group (PKOWT and PKO). $N=4$ mice for each group (MuPKOWT and MuPKO). Data are shown as mean ± SEM for each group ($n=6$). *** $P<0.001$ versus WT

evaluated. Since the changes are apparent in young adults, it is possible that they contribute to the exceptional preservation of good health at old ages in all four kinds of mice. Consistent with this idea, we have found increases in plasma GPLD1 in young adult mice that have been subjected to caloric restriction or treated with drugs that extend lifespan, including rapamycin, acarbose, 17α-estradiol, and canagliflozin [48]. Thus, increased GPLD1 in plasma is a common feature of mice destined for long lifespan, whether the increased longevity reflects a mutation (PAPP-A, Snell, Ames, GHRKO), dietary restriction, or drug. We speculate that it may be possible to use GPLD1 induction to screen for new drugs to prioritize them prior to expensive, time-consuming tests of their effects on lifespan and age-sensitive health outcomes in mice or, possibly, in humans.

The changes in adipocytes and fat-associated macrophages notable in GHRKO mice can be reproduced in mice in which GHR is disrupted in muscle cells [47], suggesting that they reflect GH-dependent regulation of muscle FNDC5 and its cleavage product irisin. We hypothesized that disruption of PAPP-A in muscle might reproduce some, or all, of the changes we had detected in global PKO mice, but the results seen in MuPKO were thoroughly unexpected and do not suggest any simple, global explanation. In the WAT depots, inguinal and perigonadal, MuPKO leads to significant changes in UCP1, Arg1, and iNOS, but they are all opposite in direction to those seen in PKO mice (and in Ames, Snell, and

GHRKO mice). Similarly, muscle FNDC5 is elevated in PKO, but depressed in MuPKO. It seems likely that the changes in FNDC5 may lead to the alterations in UCP1 and M1/M2 ratio in WAT of this series of mutant mice, but more work would be needed to test this hypothesis.

Changes in FNDC5, WAT adipocytes, and WAT-associated macrophage ratios are significant in both PKO and MuPKO mice, but in opposite directions. The changes in BAT of PKO mice, however, are not seen in the MuPKO animals, implying that control of these changes in BAT must differ, at least partly, from the control pathways in WAT. Similarly, we can conclude that the unknown pathways that upregulate FNDC5 in muscle of PKO mice must not involve direct action of PAPP-A in skeletal muscle, since muscle-specific disruption of PKO leads to significant decline in FNDC5. It is clear that FNDC5 changes in muscle must reflect contributions from PAPP-A action in at least one non-muscle cell type that remains to be identified.

Changes in BDNF and DCX, markers of neuronal health and turnover, in the brain of PKO mice are very similar to those seen in Ames, Snell, and GHRKO mice. In contrast, the alterations in brains of MuPKO seem to reflect one or more alternate PAPP-A-sensitive influences. BDNF and DCX are elevated in hippocampus of both PKO and MuPKO mice, but plasma GPLD1, thought to be a major influence on brain BDNF and DCX [49], is elevated in PKO but significantly diminished in the muscle-specific PAPP-A mutant. The hippocampus contains GPLD1 at levels that are not modulated by the elevated plasma GPLD1 in PKO mice, but MuPKO mice have a two-fold elevation of hippocampal GPLD1 that is not seen in any of the four tested long-lived varieties of mice. It is possible that local elevation of GPLD1 in hippocampus of MuPKO mice could induce the observed increase in BNDF and DCX, but this is an ad hoc speculation not yet supported by experimental data. Although GPLD1 is also produced by BAT, and shows the same elevation in PKO mice noted for liver and plasma, BAT production of GPLD1 in BAT is significantly lower in the MuPKO mice, just as it is in plasma and liver. Additional work will be needed to delineate the complex multi-cellular signaling networks that modulate GPLD1, BDNF, and DCX in brain and in peripheral tissues, but it is clear already that simple linear models, in which PAPP-A regulation of IGF1 activity explains the set of traits in the PKO mice, will not be adequate to account for the differences between PKO and MuPKO mice. The sequence of events by which GPLD1 in plasma modifies levels of BNDF and DCX in brain is, similarly, obscure and in need of detailed exploration [49].

Eukaryotic mRNAs are translated via cap-dependent and cap-independent pathways [60]. Usually, eukaryotic mRNAs are translated in a cap-dependent fashion. Under stress conditions, however, mRNA can be translated through a specific type of translation termed m6A-mediated cap-independent translation, which allows protein production from a subset of modified mRNAs only [61, 62]. Other work.

from our group has documented elevation of many CIT-regulated proteins in multiple organs of long-lived mutant mice (Snell, GHRKO), and also in tissues of mice treated with drugs that extend healthy mouse lifespan by pharmacological intervention, including rapamycin, acarbose, and 17α-estradiol [63–65]. The lifespan effect of 17α-estradiol is observed only in males [50], and its effects on selective mRNA translation by CIT are similarly sex restricted. Snell and GHRKO mice have elevated levels of YTHDF1, a protein involved in promoting CIT, and of METTL3 and METTL14, which modify the 5-UTR of selected mRNAs in ways that facilitate their translation by CIT. We have reported [48] that GPLD1 protein is increased, in culture and in mice, by interventions that upregulate CIT, such as transgenic over-expression of YTHDF1 or by use of a drug, 4-EGI1, that promotes CIT by blocking cap-dependent mRNA translation. The increase of hepatic GPLD1 protein in PKO mice, despite the absence of any effect on GPLD1 mRNA, suggests that PKO increase in GPLD1 is also likely to reflect CIT in liver, although other possible mechanisms have not been entirely ruled out. It will be of interest to determine if the decline in GPLD1 in MuPKO liver and the increase in GPLD1 in brain of MuPKO mice also reflect changes of protein independent of transcript levels. Studies of mice in which PKO is disrupted in other tissues, including liver and varieties of neurons and glial cells, may also help shed light on the way in which PAPP-A modulates local IGF1 action or, potentially, alters cell behavior in ways that do not depend on IGF1 function. Further development of animals with tissue-specific alteration of PAPP-A will help to set priorities for informative studies of

longevity in a subset of these mouse models, and thus on the pathway(s) through which global PAPP-A disruption slows aging and extends lifespan.

Our work on the PKO mice supports a growing body of evidence that long-lived mice typically have a suite of characteristics, even when evaluated as young adults, that could plausibly contribute to slowed aging and to health maintenance at older ages. This set of traits includes alterations in UCP1, macrophage subsets within adipose tissue, increased production of the myokine FNDC5/irisin that alters adipose tissue status, and production of GPLD1 and other CIT proteins in the liver, with accompanying increases in brain proteins associated with preservation of cognitive function in old age. Nearly all of these changes are also seen in genetically normal mice that have been treated with anti-aging drugs or subjected to caloric restriction [47, 48, 59]. The pathway(s) by which diminished PKO levels lead to this suite of changes are still obscure, but merit experimental attention. Our data showing that GPLD1 production within the CNS can be regulated by pathways independent of those that control GPLD1 in liver and fat should attract attention to local as well as systemic influences on GPLD1 and its targets. Assessment of GPI-anchored proteins cleaved, in brain and in various peripheral tissues, by GPLD1, and their possible effects on health-related outcomes also seems likely to generate new insights into aging and the pathology of age-related diseases. Lastly, the dramatic and unexpected set of phenotypes seen in mice with muscle-specific disruption of PAPP-A imply that the influence of this protease on pathophysiology may involve complex sets of compensatory feedback circuits that await delineation.

Acknowledgements We thank Lori Roberts, Natalie Perry, Roxann Alonzo, Jacob Sheets, and Ilkim Erturk for expert assistance in animal care. We thank Dr. Cheryl Conover for her gift of breeding stock for the PKO mutant mice. The work was supported by a grant from the Glenn Foundation for Medical Research and by NIH grants AG023122 and AG024824.

Author contribution RAM and XL conceived the experiment XL, MH, MM, ML, and RH produced the data. MS and DL provided muPKO mice and helped to characterize them. XL did the statistical analysis and prepared the figures. XL and RAM wrote the manuscript. All authors read and approved the final manuscript.

Data availability All raw images, densitometric data, and statistical calculations are available from the authors (XL, RAM) on request.

Declarations

Conflict of interest The authors declare no competing interests.

References

1. Conover CA, et al. Metalloproteinase pregnancy-associated plasma protein A is a critical growth regulatory factor during fetal development. Development. 2004;131(5):1187–94.
2. Conover CA, et al. Longevity and age-related pathology of mice deficient in pregnancy-associated plasma protein-A. J Gerontol A Biol Sci Med Sci. 2010;65(6):590–9.
3. Vallejo AN, et al. Resistance to age-dependent thymic atrophy in long-lived mice that are deficient in pregnancy-associated plasma protein A. Proc Natl Acad Sci USA. 2009;106(27):11252–7.
4. Conover CA, et al. Longevity is not influenced by prenatal programming of body size. Aging Cell. 2010;9(4):647–9.
5. Tanner SJ, et al. Impact of pregnancy-associated plasma protein-a deletion on the adult murine skeleton. J Bone Miner Res. 2008;23(5):655–62.
6. Nyegaard M, et al. Lack of functional pregnancy-associated plasma protein-A (PAPPA) compromises mouse ovarian steroidogenesis and female fertility. Biol Reprod. 2010;82(6):1129–38.
7. Conover CA, et al. Metabolic consequences of pregnancy-associated plasma protein-A deficiency in mice: exploring possible relationship to the longevity phenotype. J Endocrinol. 2008;198(3):599–605.
8. Swindell WR, Masternak MM, Bartke A. In vivo analysis of gene expression in long-lived mice lacking the pregnancy-associated plasma protein A (PappA) gene. Exp Gerontol. 2010;45(5):366–74.
9. Harrington SC, Simari RD, Conover CA. Genetic deletion of pregnancy-associated plasma protein-A is associated with resistance to atherosclerotic lesion development in apolipoprotein E-deficient mice challenged with a high-fat diet. Circ Res. 2007;100(12):1696–702.
10. Mader JR, et al. Mice deficient in PAPP-A show resistance to the development of diabetic nephropathy. J Endocrinol. 2013;219(1):51–8.
11. Ricquier D, Kader JC. Mitochondrial protein alteration in active brown fat: a soidum dodecyl sulfate-polyacrylamide gel electrophoretic study. Biochem Biophys Res Commun. 1976;73(3):577–83.
12. Inokuma K, et al. Uncoupling protein 1 is necessary for norepinephrine-induced glucose utilization in brown adipose tissue. Diabetes. 2005;54(5):1385–91.
13. Feldmann HM, et al. UCP1 ablation induces obesity and abolishes diet-induced thermogenesis in mice exempt from thermal stress by living at thermoneutrality. Cell Metab. 2009;9(2):203–9.
14. Vitali A, et al. The adipose organ of obesity-prone C57BL/6J mice is composed of mixed white and brown adipocytes. J Lipid Res. 2012;53(4):619–29.
15. Young P, Arch JR, Ashwell M. Brown adipose tissue in the parametrial fat pad of the mouse. FEBS Lett. 1984;167(1):10–4.

16. Loncar D, Afzelius BA, Cannon B. Epididymal white adipose tissue after cold stress in rats. II. Mitochondrial changes. J Ultrastruct Mol Struct Res. 1988;101(2–3):199–209.
17. Harms M, Seale P. Brown and beige fat: development, function and therapeutic potential. Nat Med. 2013;19(10):1252–63.
18. Wu J, et al. Beige adipocytes are a distinct type of thermogenic fat cell in mouse and human. Cell. 2012;150(2):366–76.
19. Boss O, Farmer SR. Recruitment of brown adipose tissue as a therapy for obesity-associated diseases. Front Endocrinol (Lausanne). 2012;3:14.
20. Wu J, Cohen P, Spiegelman BM. Adaptive thermogenesis in adipocytes: is beige the new brown? Genes Dev. 2013;27(3):234–50.
21. Exley MA, et al. Interplay between the immune system and adipose tissue in obesity. J Endocrinol. 2014;223(2):R41–8.
22. Itoh M, et al. Adipose tissue remodeling as homeostatic inflammation. Int J Inflam. 2011;2011:720926.
23. Germano G, et al. Role of macrophage targeting in the antitumor activity of trabectedin. Cancer Cell. 2013;23(2):249–62.
24. Mosser DM, Edwards JP. Exploring the full spectrum of macrophage activation. Nat Rev Immunol. 2008;8(12):958–69.
25. Murray PJ, Wynn TA. Protective and pathogenic functions of macrophage subsets. Nat Rev Immunol. 2011;11(11):723–37.
26. Lichtnekert J, et al. Changes in macrophage phenotype as the immune response evolves. Curr Opin Pharmacol. 2013;13(4):555–64.
27. Biswas SK, Mantovani A. Macrophage plasticity and interaction with lymphocyte subsets: cancer as a paradigm. Nat Immunol. 2010;11(10):889–96.
28. Grohmann U, et al. Positive regulatory role of IL-12 in macrophages and modulation by IFN-gamma. J Immunol. 2001;167(1):221–7.
29. Kraakman MJ, et al. Macrophage polarization in obesity and type 2 diabetes: weighing down our understanding of macrophage function? Front Immunol. 2014;5:470.
30. Patsouris D, et al. Insulin resistance is associated with MCP1-mediated macrophage accumulation in skeletal muscle in mice and humans. PLoS One. 2014;9(10):e110653.
31. Fuentes L, Roszer T, Ricote M. Inflammatory mediators and insulin resistance in obesity: role of nuclear receptor signaling in macrophages. Mediators Inflamm. 2010;2010:219583.
32. Costantini A, et al. Age-related M1/M2 phenotype changes in circulating monocytes from healthy/unhealthy individuals. Aging (Albany NY). 2018;10(6):1268–80.
33. Mahbub S, Deburghgraeve CR, Kovacs EJ. Advanced age impairs macrophage polarization. J Interferon Cytokine Res. 2012;32(1):18–26.
34. Ferrer-Martínez A, Ruiz-Lozano P, Chien KR. Mouse PeP: a novel peroxisomal protein linked to myoblast differentiation and development. Dev Dyn. 2002;224(2):154–67.
35. Teufel A, et al. Frcp1 and Frcp2, two novel fibronectin type III repeat containing genes. Gene. 2002;297(1–2):79–83.
36. Boström P, et al. A PGC1-α-dependent myokine that drives brown-fat-like development of white fat and thermogenesis. Nature. 2012;481(7382):463–8.
37. Huh JY, et al. FNDC5 and irisin in humans: I. Predictors of circulating concentrations in serum and plasma and II. mRNA expression and circulating concentrations in response to weight loss and exercise. Metabolism. 2012;61(12):1725–38.
38. Mazur-Bialy AI, Pochec E, Zarawski M. Anti-inflammatory properties of irisin, mediator of physical activity, are connected with TLR4/MyD88 signaling pathway activation. Int J Mol Sci. 2017;18(4):701.
39. Xiong XQ, et al. FNDC5 attenuates adipose tissue inflammation and insulin resistance via AMPK-mediated macrophage polarization in obesity. Metabolism. 2018;83:31–41.
40. Matsuo Y, et al. Fibronectin type III domain containing 5 expression in skeletal muscle in chronic heart failure-relevance of inflammatory cytokines. J Cachexia Sarcopenia Muscle. 2015;6(1):62–72.
41. Huang EJ, Reichardt LF. Neurotrophins: roles in neuronal development and function. Annu Rev Neurosci. 2001;24:677–736.
42. Francis F, et al. Doublecortin is a developmentally regulated, microtubule-associated protein expressed in migrating and differentiating neurons. Neuron. 1999;23(2):247–56.
43. Gleeson JG, et al. Doublecortin is a microtubule-associated protein and is expressed widely by migrating neurons. Neuron. 1999;23(2):257–71.
44. Mattson MP, Maudsley S, Martin B. BDNF and 5-HT: a dynamic duo in age-related neuronal plasticity and neurodegenerative disorders. Trends Neurosci. 2004;27(10):589–94.
45. Rao MS, Hattiangady B, Shetty AK. The window and mechanisms of major age-related decline in the production of new neurons within the dentate gyrus of the hippocampus. Aging Cell. 2006;5(6):545–58.
46. Shetty AK, et al. Deafferentation enhances neurogenesis in the young and middle aged hippocampus but not in the aged hippocampus. Hippocampus. 2011;21(6):631–46.
47. Li X, et al. Muscle-dependent regulation of adipose tissue function in long-lived growth hormone-mutant mice. Aging (Albany NY). 2020;12(10):8766–89.
48. Li X, et al. Cap-independent translation of GPLD1 enhances markers of brain health in long-lived mutant and drug-treated mice. Aging Cell. 2022;21:e13685.
49. Horowitz AM, et al. Blood factors transfer beneficial effects of exercise on neurogenesis and cognition to the aged brain. Science. 2020;369(6500):167–73.
50. Shen Z, et al. Cap-independent translation: a shared mechanism for lifespan extension by rapamycin, acarbose, and 17α-estradiol. Aging Cell. 2021;20(5):e13345.
51. Dominick G, et al. mTOR regulates the expression of DNA damage response enzymes in long-lived Snell dwarf, GHRKO, and PAPPA-KO mice. Aging Cell. 2017;16(1):52–60.
52. Conover CA, Bale LK, Powell DR. Inducible knock out of pregnancy-associated plasma protein-a gene expression in the adult mouse: effect on vascular injury response. Endocrinol. 2013;154(8):2734–8.

53. Dun SL, et al. Irisin-immunoreactivity in neural and non-neural cells of the rodent. Neurosci. 2013;240:155–62.
54. Wrann CD. FNDC5/irisin - their role in the nervous system and as a mediator for beneficial effects of exercise on the brain. Brain Plast. 2015;1(1):55–61.
55. Liu P, et al. Quercetin ameliorates hypobaric hypoxia-induced memory impairment through mitochondrial and neuron function adaptation via the PGC-1α pathway. Restor Neurol Neurosci. 2015;33(2):143–57.
56. Sun LY, Bartke A. Adult neurogenesis in the hippocampus of long-lived mice during aging. J Gerontol A Biol Sci Med Sci. 2007;62(2):117–25.
57. Kinney BA, et al. Evidence that Ames dwarf mice age differently from their normal siblings in behavioral and learning and memory parameters. Horm Behav. 2001;39(4):277–84.
58. Sharma S, et al. NMDA and kainate receptor expression, long-term potentiation, and neurogenesis in the hippocampus of long-lived Ames dwarf mice. Age (Dordr). 2012;34(3):609–20.
59. Li X, et al. Transient early life growth hormone exposure permanently alters brain, muscle, liver, macrophage, and adipocyte status in long-lived Ames dwarf mice. FASEB J. 2022;36(7):e22394.
60. Shatsky IN, et al. Cap-independent translation: what's in a name? Trends Biochem Sci. 2018;43(11):882–95.
61. Meyer KD, et al. 5' UTR m(6)A promotes cap-independent translation. Cell. 2015;163(4):999–1010.
62. Zhou J, et al. Dynamic m(6)A mRNA methylation directs translational control of heat shock response. Nature. 2015;526(7574):591–4.
63. Wilkinson JE, et al. Rapamycin slows aging in mice. Aging Cell. 2012;11(4):675–82.
64. Harrison DE, et al. Acarbose, 17-α-estradiol, and nordihydroguaiaretic acid extend mouse lifespan preferentially in males. Aging Cell. 2014;13(2):273–82.
65. Strong R, et al. Longer lifespan in male mice treated with a weakly estrogenic agonist, an antioxidant, an α-glucosidase inhibitor or a Nrf2-inducer. Aging Cell. 2016;15(5):872–84.